Observation of an electromagnetically induced grating in cold sodium atoms

Masaharu Mitsunaga and Nobuyuki Imoto
NTT Basic Research Laboratories, Atsugi-shi, Kanagawa 243-0198, Japan
(Received 31 December 1998)

We have observed diffraction signals by a grating originating from electromagnetically induced transparency (EIT) in a three-level Λ system of cold sodium atoms. Theoretical and experimental analyses of this phenomenon, called the electromagnetically induced grating (EIG), have revealed that EIG spectra exhibit background-free, Lorentzian signal profiles regardless of the pump frequencies, making a clear contrast to the case of ordinary EIT spectra. [S1050-2947(99)06306-4]

PACS number(s): 42.50.Gy, 32.80.Pj, 42.50.Md

In a three-level system, absorption of a probe beam is nullified in the presence of a pump beam which couples the common excited state to a third level. This quenching of absorption, well known as electromagnetically induced transparency (EIT) [1], is observed as a dip in the probe absorption spectrum. So far these dip signals have been mainly observed in room-temperature gaseous samples [1,2], i.e., inhomogeneous systems. They have also been observed in homogeneous systems like cold neutral atoms [3,4], because the dip widths can become even narrower than homogeneous linewidths. Phenomenologically speaking, EIT is quite analogous to the spectral hole burning (SHB) [5] where again a probe absorption is reduced by a strong pump beam, although the mechanisms of SHB and EIT are intrinsically different [6]. In SHB, basically, two types of detection schemes have been developed to monitor the pump-induced dips. One is transmission and the other is called holographic readout [7,8], in which the pump-induced spatially periodic hole pattern is monitored by the probe diffraction. This technique can be transferred to EIT, and it was theoretically proposed by the name of electromagnetically induced grating (EIG) [9].

EIG can be explained in Fig. 1, taking cold Na atoms for an example. As shown in Fig. 1(a), a pair of pump beams (pump no. 1 and pump no. 2) and a probe beam intersect in the cold atom cloud. The pump (=coupling) frequency ω_c and the probe frequency ω_p connect the $3S_{1/2}$ ground-state $F=2$ and 1 levels, respectively, to the $3P_{3/2}$ excited states as shown in Fig. 1(b). Because of the interference pattern created by the pump beams, in the bright fringes the medium becomes transparent due to EIT, while in the dark fringes the medium is still opaque. This type of absorption grating (EIG) should diffract the probe beam. Therefore one monitors EIT for the probe transmission spectrum and EIG for the probe diffraction spectrum as illustrated in Fig. 1(a). The advantages of EIG over EIT should be inferred from those of holographic readout over transmission readout in SHB. Since there is no background in EIG, it gives much higher sensitivity, whereas EIT signals may be easily hidden in noisy absorption spectra for smaller pump intensities. Also, in EIG the nonlinear polarization signal is monitored as its intensity, not as a real or imaginary part, and the identification of the signal is very easy. On the other hand, EIT signals show very complex line shapes, as we will see later. In a solid-state material EIG has already been reported by Ham and coworkers [10]. However, their results are quite different from our case both theoretically and experimentally, due to the nature of the inhomogeneously broadened medium. In this paper we report on the observation of EIG signals in cold Na atoms and check the above-mentioned advantages for EIG.

We have developed a perturbative approach [11,12] to this problem. We consider a quasi-three-level system where the ground-state $F=1$ level (denoted as 1) and the $F=2$ level (denoted as 2) and one of the excited-state $F'=j$ levels ($j=0$, 1, or 2) (denoted as j or k) form a three-level system [see Fig. 1(b)]. What we want to obtain is the third-order nonlinear optical polarization p_{NL}, or optical coherence ρ_{1j} or ρ_{2j} starting from the ground-state populations ρ_{11} and ρ_{22}. By solving the equation of motion for the density matrix for this homogeneous medium, we obtain 32 terms corresponding to 32 elementary processes for p_{NL}. These pro-

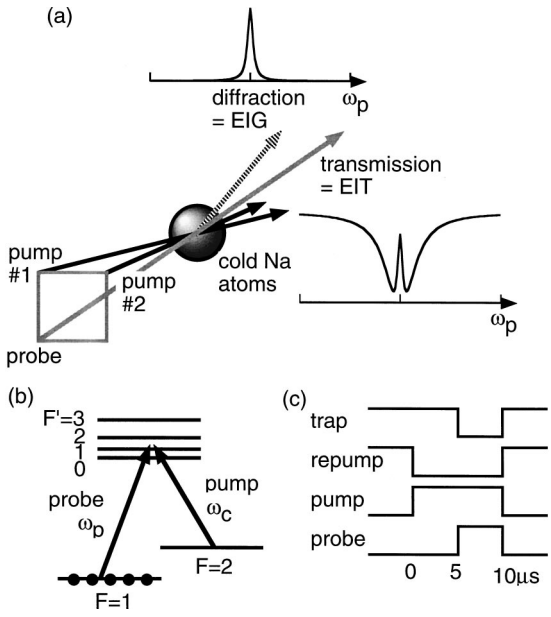

FIG. 1. (a) Beam configuration and expected spectra in EIT and EIG experiments. EIT monitors the transmission of the probe beam with the presence of the pump beams, whereas EIG monitors the Bragg diffraction of the probe beam from the pump-induced grating. The trap and repump beams are omitted. (b) The energy level diagram of the Na atom. The population is in the $F=1$ dark level in our theoretical and experimental framework. (c) Experimental pulse-timing sequence of the trap, repump, pump, and probe beams.

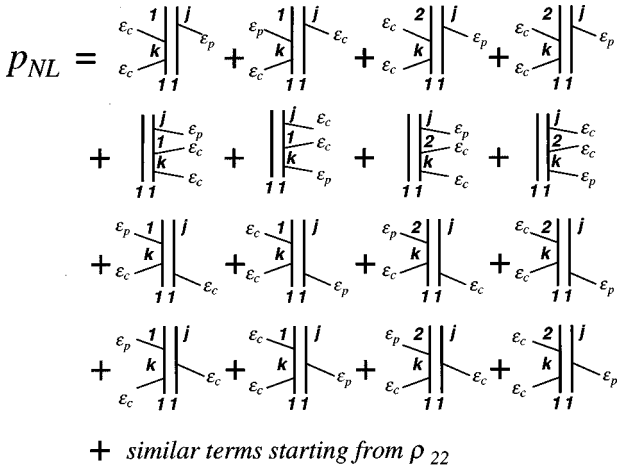

FIG. 2. Double Feynman diagrams showing 32 elementary processes contributing to the third-order nonlinear optical polarization. The remaining 16 diagrams starting from ρ_{22} are not shown but are obtained by simply replacing 11 at the bottom of each diagram by 22.

cesses can be most easily understood by using double Feynman diagrams [13,14] as illustrated in Fig. 2. By considering the case where the population is mainly in level 1, those starting from ρ_{22} are all neglected. Besides, since ω_c and ω_p are nearly resonant to the $2-j$ and $1-j$ transitions (note that the ground-state hyperfine splitting $\sim$1.77 GHz is much larger than the excited-state splittings $\sim$60, 34, and 16 MHz), respectively, only one term (the eighth term in Fig. 2) out of 32 terms can contribute to p_{NL} and is written in the form

$$p_{\mathrm{NL}}=\frac{i}{\hbar^3}\varepsilon_p\varepsilon_c^2\frac{1}{i(\omega_p-\omega_c-\omega_{21})+\gamma_{12}} \times\sum_{k,j}\frac{p_{1k}p_{k2}p_{2j}p_{j1}}{\{i(\omega_p-\omega_{k1})+1/T_2\}\{i(\omega_p-\omega_{j1})+1/T_2\}}, \tag{1}$$

where $\varepsilon_p(\varepsilon_c)$ is the laser field amplitude of the probe (pump) beam and ω_{lm} is the splitting frequency between the levels l and m. T_2 is the dephasing time of the optical transition which is common for both the optical transitions, γ_{12} is the sublevel dephasing rate, and $p_{j1}(p_{j2})$ is the optical dipole moment for the $F=1$ $(F=2)$ to $F'=j$ transition. The ordinary linear polarization p_L for the probe beam, on the other hand, is simply given as

$$p_L=-\frac{i}{\hbar}\varepsilon_p\sum_j\frac{p_{j1}^2}{i(\omega_p-\omega_{j1})+1/T_2}. \tag{2}$$

By using these expressions (1) and (2), three different types of signal profiles, ordinary transmission, EIT, and EIG, can be obtained as a function of ω_p, denoted as S_{tr}, S_{EIT}, and S_{EIG}, respectively. By neglecting the propagation effect, S_{tr}, S_{EIT}, and S_{EIG} are expressed as

$$S_{\mathrm{tr}}=\mathrm{Im}[p_L], \tag{3}$$

$$S_{\mathrm{EIT}}=\mathrm{Im}[p_L+p_{\mathrm{NL}}], \tag{4}$$

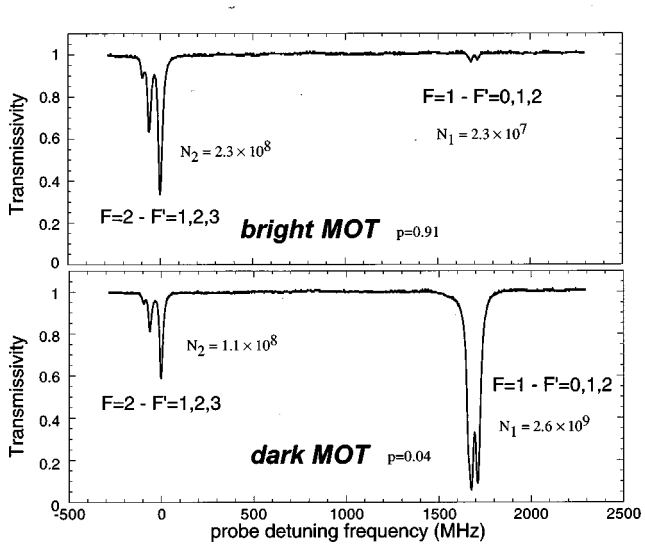

FIG. 3. Transmission spectra for the $F=2$ to $F'=1$, 2, and 3 transitions (left) and $F=1$ to $F'=0$, 1, and 2 transitions (right) of cold Na atoms for the bright MOT (upper trace) and the dark MOT (lower trace) configurations. The numbers of atoms in $F=1$ level (N_1) and $F=2$ level (N_2) are calculated from the spectra and are shown in the figure, considering that the size of the cloud is 3 mm in diameter. Also shown are the ratios $p=N_2/(N_1+N_2)$ for the two MOTs.

$$S_{\mathrm{EIG}}=|p_{\mathrm{NL}}|^2, \tag{5}$$

where Im[...] represents the imaginary part. It should be mentioned that, although p_{NL} expressed by Eq. (1) is composed of many complex Lorentzians, the first Lorentzian peaked at $\omega_p=\omega_c+\omega_{21}$ with width γ_{12} gives the signal profile since $\gamma_{12}\ll 1/T_2$. However, the phase of this profile will be dependent on the remaining factor. Since EIT takes the imaginary part of p_{NL}, the signal exhibits a positive or negative Lorentzian or dispersion curve depending on the phase, or on the pump frequency. This issue will be discussed in detail later. In the EIG signal, however, the absolute value of p_{NL} is taken and the signal profile is always a simple Lorentzian. It is also worthwhile to notice that Eq. (1) can be regarded as a resonant stimulated Raman scattering signal originating from a sublevel coherence. In this sense EIT can be interpreted as the interference of the linear process and the stimulated Raman process while EIG is a pure stimulated Raman process.

On the experimental side, a cold Na atom cloud was prepared in a manner similar to that described by our previous work [15]. This time, however, a dark magneto-optical trap (MOT) has been employed [16] by making a dark spot of $\sim$5 mm in diameter inside the repumping beam profile. The transmission spectra of dark and bright MOTs in our experiment are shown in Fig. 3. In the bright MOT the $F=2$ to $F'=1,2,3$ curve (left feature) is much more pronounced than the $F=1$ to $F'=0,1,2$ curve (right feature), indicating that most atoms (91%) populate in the bright $F=2$ level. In contrast, in the dark MOT 96% of the atoms are in the dark $F=1$ level. Besides, by employing the dark MOT the total number of trapped atoms increased about a factor of 10 compared to the bright MOT case, as shown in Fig. 3. These findings imply that the dark MOT configuration is an ideal

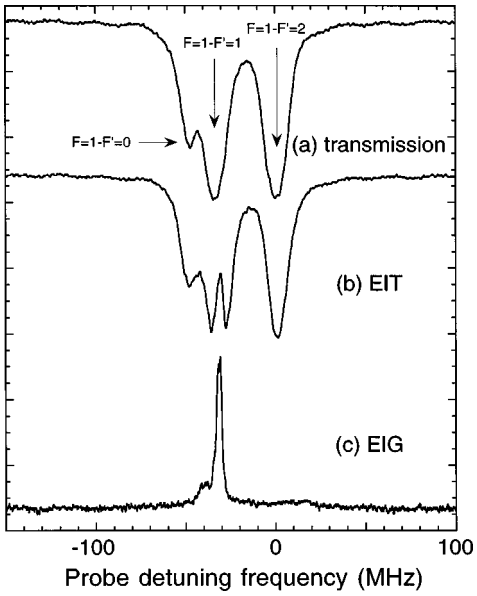

FIG. 4. (a) Transmission, (b) EIT, and (c) EIG spectra for the $F=1$ to $F'=0$, 1, and 2 transitions of cold Na atoms. Pump frequency was resonant to the $F=2-F'=1$ transition.

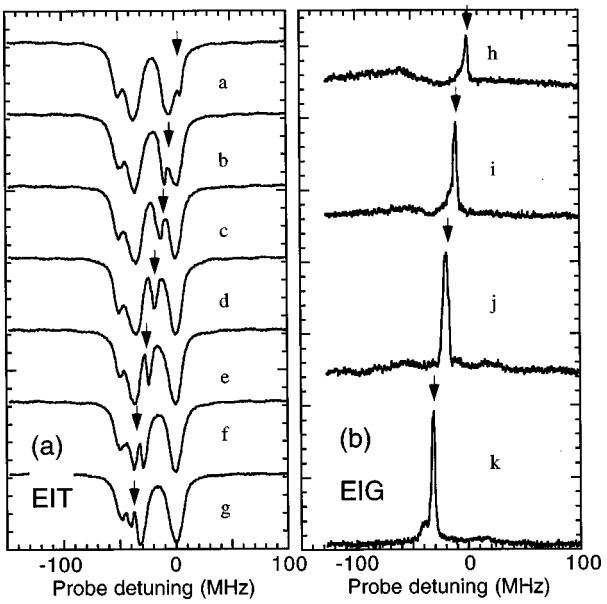

FIG. 5. Pump frequency dependence of (a) EIT and (b) EIG spectra. The arrow in each trace indicates the position corresponding to $\omega_c+\omega_{21}$.

system for studying EIT and EIG, where the deeply populated $F=1$ level is used as the monitor level for the probe laser and the almost-empty $F=2$ level is used as the third level coupled by the pump laser. After preparation of dark MOT, the trap and repump pulses were switched off and a pair of pump pulses and a probe pulse were applied. The pulse timing sequence is shown in Fig. 1(c). All the beams but the probe beam were provided from the same laser source (single frequency ring dye laser operating at ~589 nm) by acousto-optic modulators, whereas the probe beam was derived from an independent ring dye laser. This allowed smooth scanning of the probe frequency with wide scan range and constant probe intensity. The diffracted signal could be identified by a charge-coupled device (CCD) camera. More quantitatively, the transmitted (EIT) and the diffracted (EIG) signal intensities of the probe pulse (power~60 nW for EIT and 300 μW for EIG) as a function of the probe frequency were detected by photomultiplier tubes, averaged by boxcar integrators, and displayed in a digitizing oscilloscope. This type of coherent four-wave mixing signals should be distinguished from incoherent four-wave mixing signals as we reported previously [15], where hyperfine population grating is created by the pump pulses, which persist a long time (~10 μs). To check this, we plotted the EIG signal intensity as a function of the probe delay time. The signal was observed only when the pump pulse and the probe pulse were temporally overlapped. This finding is contrary to Ref. [15] and shows that the laser-induced grating is not long-lived and the hyperfine population grating can be neglected.

The three signal profiles, i.e., transmission, EIT, and EIG, are shown in Fig. 4, for the common probe detuning frequency axis. In the transmission spectrum, the hyperfine transitions from the ground $F=1$ to the excited $F'=0$, 1, and 2 transitions are partially resolved, since the the hyperfine splitting frequencies (34 and 16 MHz) are comparable to the natural linewidth (10 MHz) of the Na atom. When the pump pulse with frequency corresponding to the $F=2$ to $F'=1$ transition is applied, the transmission spectrum is modified and an EIT profile is clearly seen [Fig. 4(b)] as a dip at the $F=1-F'=1$ absorption peak. The width of the dip was limited by the laser linewidth but can be much narrower. An EIG signal profile was obtained by monitoring the diffraction intensity instead of transmission and shown in Fig. 4(c). Here a simple single peak is observed at the same position and the same width as that of EIT but without background.

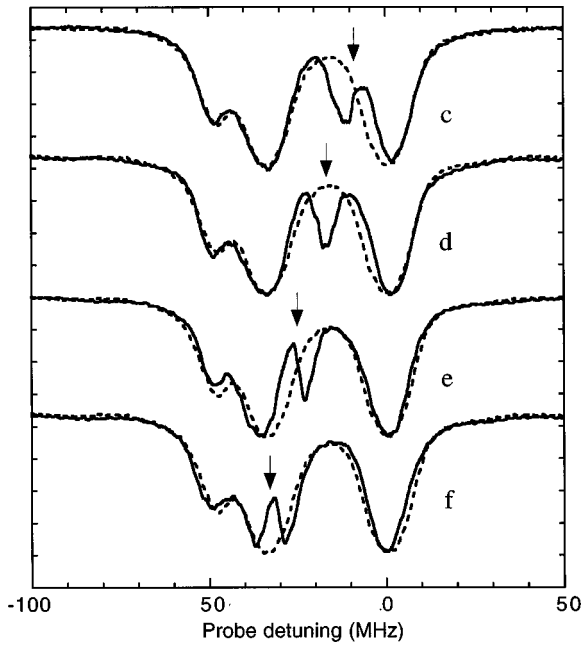

FIG. 6. EIT curves *c*, *d*, *e*, and *f* of Fig. 5 (solid lines) superposed on the transmission spectra (broken lines) to emphasize the differences of the two spectra. The arrow in each trace indicates the position corresponding to $\omega_c+\omega_{21}$.

The behavior of the signal profiles for various pump frequencies ω_c was investigated for EIT and EIG, as shown in Fig. 5. The positions corresponding to $\omega_c+\omega_{21}$ are indicated by the arrows. As mentioned before the EIT signal profile changes its phase depending on ω_c. This behavior is more clearly seen in Fig. 6, which is a magnified version of Fig. 5(a) superposed on the transmission curves. At the points of peak absorption [curve *f* of Fig. 5(a) and Fig. 6 or curve *b* of Fig. 5(a)], the EIT signals show upward Lorentzian (transparency). On the other hand, in the middle of the two absorption peaks (curve *d*) it becomes downward Lorentzian (extra absorption). And at the positions in between (curves *c* and *e*) they show dispersion-type behavior. This behavior indeed agrees with the above-mentioned theory. In fact, we rewrite S_{EIT} in Eq. (4), by using Eq. (1), as

$$S_{\mathrm{EIT}}=\mathrm{Im}[p_L]+\mathrm{Im}\left[\frac{i}{i(\omega_p-\omega_c-\omega_{21})+\gamma_{12}}\mathrm{Re}^{i\theta}\right], \quad (6)$$

where $\mathrm{Re}^{i\theta}$ is defined as

$$\mathrm{Re}^{i\theta}\equiv\frac{\varepsilon_p\varepsilon_c^2}{\hbar^3}\frac{p_{1e}^2p_{2e}^2}{\{i(\omega_c+\omega_{21}-\omega_{e1})+1/T_2\}^2}, \quad (7)$$

and θ determines the phase part of the function. Here we assumed only one excited-state level denoted as *e* for simplicity and the function in Eq. (7) was evaluated at $\omega_p=\omega_c+\omega_{21}$ since it is smoothly varying around that point. From Eq. (7) it is clear that, depending on the case where the EIT signal is (i) right at the peak absorption ($\omega_c+\omega_{21}=\omega_{e1}$), (ii) at the right wing of the absorption ($\omega_c+\omega_{21}\sim\omega_{e1}+1/T_2$), (iii) at the left wing of the absorption ($\omega_c+\omega_{21}\sim\omega_{e1}-1/T_2$), and (iv) far off resonance ($\omega_c+\omega_{21}\sim\omega_{e1}\pm\alpha$ where $\alpha\gg 1/T_2$), θ takes the value of (i) 0, (ii) $-\pi/2$, (iii) $\pi/2$, and (iv) π. By substituting these results into Eq. (6), we obtain the EIT profiles as (i) upward Lorentzian (curve *f*), (ii) dispersive curve with negative slope at the center (curve *e*), (iii) dispersive curve with positive slope at the center (curve *c*), and (iv) downward Lorentzian (curve *d*). In contrast to the EIT case, EIG signals [Fig. 5(b)] always exhibit simple Lorentzians right at the positions of $\omega_c+\omega_{21}$. Only the peak magnitudes vary depending on $\omega_c+\omega_{21}$.

In summary, we have developed a perturbation theory for a type of detection scheme for EIT, or EIG, which employs nearly degenerate four-wave mixing to allow a background-free measurement of EIT. The experimental demonstration by using a cold Na atom sample indeed supported the theoretical predictions. This type of high-sensitivity measurement mitigates the requirement of high pump intensities which causes the saturation effect, and is particularly suitable for the investigation of the ultimate signal linewidth γ_{12} that should be extremely narrow.

The authors are grateful for helpful discussions with Dr. Makoto Yamashita and Dr. Masato Koashi.

[1] K.-J. Boller, A. Imamoglu, and S. E. Harris, Phys. Rev. Lett. **66**, 2593 (1991); J. E. Field, K. H. Hahn, and S. E. Harris, *ibid.* **67**, 3062 (1991); A. Kasapi, M. Jain, G. Y. Yin, and S. E. Harris, *ibid.* **74**, 2447 (1995).

[2] Y. Li and M. Xiao, Phys. Rev. A **51**, 4959 (1995); Y. Li, S. Jin, and M. Xiao, *ibid.* **51**, R1754 (1995); Y. Li and M. Xiao, Opt. Lett. **21**, 1064 (1996); A. M. Akulshin, S. Barreiro, and A. Lezama, Phys. Rev. A **57**, 2996 (1998).

[3] M. Mitsunaga, T. Mukai, K. Watanabe, and T. Mukai, J. Opt. Soc. Am. B **13**, 2696 (1996).

[4] N. Shiokawa, Y. Torii, T. Hirano, and T. Kuga (unpublished); S. A. Hopkins, E. Usadi, H. X. Chen, and A. V. Durrant, Opt. Commun. **138**, 185 (1997); A. V. Durrant, H. X. Chen, S. A. Hopkins, and J. A. Vaccaro, *ibid.* **151**, 136 (1998).

[5] *Persistent Spectral Hole-Burning: Science and Applications*, edited by W. E. Moerner, Topics in Current Physics Vol. 44 (Springer-Verlag, Berlin, 1988).

[6] First, SHB has a signal dip corresponding to the homogeneous linewidth within the inhomogeneously broadened spectrum. In EIT, on the other hand, even within the homogeneous broadening a very narrow dip is observed. Secondly, since SHB is an incoherent four-wave mixing, the hole spectrum often lasts very long even after the pump pulse is switched off. In contrast, in EIT, which is a coherent four-wave mixing, the dip spectrum will return to the original transmission spectrum as soon as the pump beam is switched off.

[7] A. Renn, A. Meixner, U. P. Wild, and F. A. Burkhalter, Chem. Phys. **93**, 157 (1985).

[8] M. Mitsunaga, N. Uesugi, H. Sasaki, and K. Karaki, Opt. Lett. **19**, 752 (1994).

[9] H. Y. Ling, Y. Li, and M. Xiao, Phys. Rev. A **57**, 1338 (1998).

[10] B. S. Ham, M. S. Shahriar, and P. R. Hemmer, Opt. Lett. **22**, 1138 (1997); B. S. Ham, M. S. Shahriar, M. K. Kim, and P. R. Hemmer, *ibid.* **22**, 1849 (1997).

[11] M. Mitsunaga, N. Uesugi, and K. Sugiyama, Opt. Lett. **18**, 1256 (1993).

[12] M. Mitsunaga and R. G. Brewer, Phys. Rev. A **32**, 1605 (1985).

[13] Y. R. Shen, *The Principles of Nonlinear Optics* (Wiley-Interscience, New York, 1984).

[14] M. Mitsunaga, R. Yano, and N. Uesugi, Phys. Rev. B **45**, 12 760 (1992).

[15] M. Mitsunaga, M. Yamashita, M. Koashi, and N. Imoto, Opt. Lett. **23**, 840 (1998).

[16] W. Ketterle, K. B. Davis, M. A. Joffe, A. Martin, and D. E. Pritchard, Phys. Rev. Lett. **70**, 2253 (1993).